Mechanism and Machine Theory 96 (2016) 165–178

Contents lists available at ScienceDirect

Mechanism and Machine Theory

journal homepage: www.elsevier.com/locate/mechmt

Stiffness analysis of a 2-DoF over-constrained RPM with an articulated traveling platform

Tao Sun, Binbin Lian, Yimin Song *

Key Laboratory of Mechanism Theory and Equipment Design of Ministry of Education, Tianjin University, Tianjin 300072, China

ARTICLE INFO

Article history:
Received 4 February 2015
Received in revised form 29 September 2015
Accepted 30 September 2015
Available online 11 November 2015

Keywords:
2-DoF over-constrained rotational parallel mechanism
Articulated traveling platform
Stiffness model
Gravitational effects
n-DoF virtual spring

ABSTRACT

Driven by the requirements of inter-satellite link antenna for tracking mechanism with two degree-of-freedom (DoF), this paper proposes a 2-DoF over-constrained rotational parallel mechanism (RPM) with an articulated traveling platform and formulates its stiffness model considering gravitational effects. The stiffness modeling is implemented by three steps: 1) Considering the over-constrained property and gravitational effects, twist/wrench mapping models of two $\underline{R}(RU)^2$ limbs connecting the fixed base and the articulated traveling platform are obtained based upon screw theory. 2) Employing deformation superposition principle, the compliance models of two $\underline{R}(RU)^2$ limbs in their joint spaces are formulated, of which component compliance is described by *n*-DoF ($n \le 6$) virtual springs; and 3) by applying deformation compatibility conditions and twist/wrench mapping models into the virtual work equations, the stiffness model of the 2-DoF over-constrained RPM considering gravitational effects is derived. From component, limbs to mechanism, the stiffness modeling process demonstrates their relations with clear physical meaning and unifies performances including kinematic, stiffness, accuracy and dynamics. This approach is verified by commercial FEA software. Finally the stiffness distribution and gravitational effects within prescribed workspace are discussed.

1. Introduction

The inter-satellite link antenna of the tracking and data relay satellite (TDRS) needs to track the satellite and receive the signal in real time, and the tracking operation is usually carried out by the tacking mechanism having two rotational degrees-of-freedom (DoFs) [1–3]. The traditional tracking mechanism is to employ the serial topology structure with two shafts connected perpendicularly, such as the famous COMETS tracking mechanism [1]. However, with the expansion of aperture and the increment of antenna weight, it is inevitable to design the tracking mechanism with serial topology structure towards larger size and heavier weight, which cannot be allowed due to the limitation of the satellite space and weight [2,3]. In addition, stiffness, accuracy and velocity performances are the disadvantages of this serial tracking mechanism [4,5]. Bearing these in mind, the tracking mechanisms with parallel topology structure have drawn more and more attention from both academia and industry in recent years.

In this paper, the tracking mechanism with parallel topology structure is referred to as the 2-DoF rotational parallel mechanism (RPM) which has been intensively investigated over the past few decades. The 5R mechanism is claimed as the simplest topology structure of the 2-DoF RPMs, in which R denotes the revolute joint and the axes of these revolute joints intersect at common point [6–8]. By introducing parallelogram structure, Baumann et al. [9] invented a 2-DoF RPM called Pantoscope that has been applied to the micro invasive surgery. Inspired by human wrist, Ross–Hime Designs [10] proposed a 2-DoF RPM named as Omni Wrist, whose performance was investigated by Sdfka et al. [11–13]. After that, Carricato and Parenti-Castelli [14] applied interconnected slider–

* Corresponding author. Tel./fax: +86 22 87402015.
E-mail address: ymsong@tju.edu.cn (Y. Song).

http://dx.doi.org/10.1016/j.mechmachtheory.2015.09.008
0094-114X/

crank linkages to formulate decoupled 2-DoF RPM. Di Gregorio and Sinatra [15] employed two PUS kinematic chains and one U joint for the 2-DoF pointing mechanism. Herein, P, U, and S denote actuated prismatic joint, universal joint and spherical joint, respectively. Furthermore, Vertechy and Parenti-Castelli [16] proposed synthesis approach of 2-DoF fully RPM with US leg. Based upon the graphic approach, Yu et al. [17,18] investigated a type of 2-DoF RPM with equal-diameter spherical pure rotation. In addition, Gogu [19] designed a 2-DoF uncoupled RPM with isotropy based on the condition number of Jacobian matrix. Recently, Cammarata [20] reconsidered the topology of U-2PUS for solar tracking system and conducted its optimized design.

While 2-DoF RPMs with larger rotational angles, better stiffness and accuracy performances are needed, it is concluded from the above-mentioned literatures that the existing topology structures of 2-DoF RPMs are difficult to meet the increasing demands in satellite tracking mechanism, as well as in aerospace, military and biomimetic fields. This paper proposes a promising solution for these demands, a 2-DoF over-constrained RPM with an articulated traveling platform, which has the potential of large rotational angles, good stiffness and superior accuracy [21–23]. Noting that good stiffness performance of the tracking mechanism provides fundamental guarantee for achieving accurate tracking, i.e., accuracy performance of 2-DoF RPM, stiffness is the key concern in this paper.

Stiffness modeling and analysis are two basic and crucial procedures of stiffness design and estimation in preliminary and final design of parallel mechanisms. As an over-constrained parallel mechanism, its over-constrained property can provide linear dependent constraints to enhance the capacity resisting external payloads and do not change the DoF of the mechanism. For this reason, there are several differences between the stiffness modeling of over-constrained and non-over-constrained parallel mechanisms. Literature reviews [24–32] show that there are three main methods for stiffness modeling of over-constrained parallel mechanisms: finite element analysis (FEA) approach, structural matrix approach, and virtual joint approach.

The FEA approach is regarded as the most accurate and reliable approach to formulate the stiffness model of over-constrained parallel mechanisms, in which the components with irregular shape can be modeled precisely [24,25]. However, the stiffness mapping between joint space and operated space cannot be expressed analytically. Besides, the FEA models have to be re-meshed and recomputed as configuration of end-effector changes, which will increase the computational costs. In consequence, the FEA approach is not suitable for parameterized stiffness model. It is usually utilized to the stiffness estimation in the preliminary design stage and the stiffness verification in the final design stage.

The structure matrix approach is to employ standard elements such as beam, shell and plate elements to describe the stiffness matrix of components then assemble to form the stiffness matrix of whole mechanism by compatibility conditions [24–28]. Comparing to FEA approach, structure matrix approach is able to derive analytical stiffness model no matter how complex the over-constrained parallel mechanism is. However, Pashkevich [25] reminded that the structural matrix approach is more complicated in computing multi-dimensional matrix thus not suitable for stiffness design of parallel mechanisms. In addition, the stiffness matrices of standard elements are not accurate to characterize the stiffness of actual components with irregular shape.

The virtual joint approach provides acceptable accuracy with lower computational efforts comparing with the approaches mentioned above, and it has been widely used in analytical parametric analysis of both over-constrained and non-over-constrained parallel mechanisms in the light of Jacobian matrix and virtual work principle. Unlike non-over-constrained parallel mechanisms, the Jacobian matrix of over-constrained parallel mechanism cannot directly apply to compute stiffness model because of the over constrained condition. Bearing this in mind, Majou [30] appended three additional virtual springs to describe the over-constrained condition of Orthoglide mechanism with parallelogram-type legs while he proposed an elimination method to achieve the stiffness matrix with virtual joint approach. However, Pashkevich [25] believed that additional virtual joints changed the mechanism structure and then established the stiffness model of Orthoglide mechanism by employing 6-DoF virtual springs to describe component and joint stiffness. With the 6-DoF generalized spring, Taghvaeipour [31] developed elestostatic analysis method for mechanical systems, including over-constrained manipulator. It is found out that 6-DoF virtual springs are suitable for accurate and complete stiffness model of over-constrained parallel mechanism, but it consists of redundant springs since linear or angular stiffness of some components corresponding movable axis is zero, which might need to be paid extra effort for dealing with the redundant stiffness of virtual spring.

What's more, even though the microgravity environment of outer space results in the invalidation of gravity of the 2-DoF tracking mechanism, it is noting that the 2-DoF tracking mechanism will be estimated and verified repeatedly on the earth before launching to outer space. Therefore, the gravity of the 2-DoF tracking mechanism needs to be considered in the stiffness model for analyzing its effect separately.

As is known to all, Jacobian matrix, reflecting the wrench/twist relationship between limbs and mechanism, is an important operator for the analysis of parallel mechanism in terms of the kinematic, stiffness, accuracy and dynamic performance. Bearing aforementioned issues in mind, on the basis of the conventional Jacobian matrix, the wrench/twist mapping model of each limb and the 2-DoF RPM is taken into account separately, allowing the consideration of the over-constraints and external wrench such as gravity. And the stiffness/compliance of every limb is computed by the sum of component deformations described by n-DoF spring ($n \le 6$), concerning the effect of passive joints. The component deformations are obtained from the FEA software, making it more reliable and accurate. By the three steps from component, limbs to the 2-DoF RPM, the stiffness model is achieved with clear physical meaning and helps to unify mechanism performance analysis including kinematic, stiffness, accuracy and dynamic.

Having outlined in Section 1 the state of the art, existing problems and the promising solutions for the stiffness of 2-DoF over-constrained RPMs, the paper is organized as follows. In Section 2, the RPM description and inverse position analysis are introduced briefly. The stiffness model considering gravitational effect is formulated in Section 3 after obtaining the twist and wrench mapping modes. In Section 4, the stiffness matrices of two linked limbs are obtained utilizing n-DoF ($n \le 6$) virtual spring approach. Section 5 demonstrates the determination of the component compliance in detail. A typical example is then given in Section 6 to verify the stiffness modeling process before the conclusions are drawn in Section 7.

2. Mechanism description and inverse position analysis

As shown in Fig. 1, the proposed 2-DoF over-constrained RPM is consist of a fixed base, two $\underline{\mathrm{R}}(\mathrm{RU})^2$ limbs and an articulated traveling platform. Herein, $\underline{\mathrm{R}}$ denotes the actuated revolute joint. The $\underline{\mathrm{R}}(\mathrm{RU})_2$ limb connects the fixed base by $\underline{\mathrm{R}}$ joint and links the plate I or plate II by two U joints. More specifically, the 1st (3rd) rod and the 2nd (4th) rod link the 1st (2nd) bracket and plate I (plate II) by R joint and U joint, respectively. The plate I and plate II are articulated by one R joint to form the articulated traveling platform shown in Figs. 1 and 2, in which the plate I is regarded as the output end of motion/force and connected rigidly to the end-effector. The introduction of an articulated traveling platform can enlarge rotational angles of the 2-DoF RPM effectively and decrease the geometrical constraints dramatically.

As shown in Fig. 2, one axis of the U joint is collinear with that of the other U joint in the same $\underline{\mathrm{R}}(\mathrm{RU})^2$ limb, meanwhile the other axes are parallel to the axes of R joints that perpendicular to the plane of the $\underline{\mathrm{R}}(\mathrm{RU})^2$ limb. The axis of $\underline{\mathrm{R}}$ joint is parallel to axes of R joints in same $\underline{\mathrm{R}}(\mathrm{RU})^2$ limb. Point A_1, A_2, B_1 and B_2 denote the centers of R joints, while point A_3, A_4, B_3 and B_4 denote the centers of U joints, respectively. C_1 and C_2 represent the centers of $\underline{\mathrm{R}}$ joints. The intersection points of two $\underline{\mathrm{R}}(\mathrm{RU})^2$ limbs within the planes of the fixed base and the articulated traveling platform are designed as point O and D, respectively.

In order to describe the motions of the 2-DoF RPM, a fixed reference frame designated as frame $O-xyz$ is assigned to the point O with the z-axis coincident with the intersection line of the two $\underline{\mathrm{R}}(\mathrm{RU})^2$ limbs and x-axis pointing to C_2, whereas a moving reference frame $D-uvw$ is established at point D, its u-axis is collinear with A_4A_3 and the w-axis is normal to the plane of the articulated traveling platform. A local reference frame $D-u_1v_1w_1$ is defined at point D whose u_1-axis points to the same direction as u-axis and v_1-axis is collinear with y-axis. Similarly, a local reference frame $D-u_2v_2w_2$ is located at point D with u_2-axis pointing to C_2 and $\bar{v}_2$-axis coincident with B_4B_3. An instantaneous reference frame $D-x'y'z'$ is defined at point D, whose axes are parallel with those of frame $O-xyz$ at home configuration. In addition, by rotating angle $\varphi(\varphi=-5\pi/4)$ about z-axis of frame $O-xyz$, the gravitational reference frame $O-x_gy_gz_g$ is established whose x_g-axis is collinear with the direction of gravity acceleration (see Fig. 3).

Based upon the above-mentioned definitions, the orientation matrices $\boldsymbol{R}_1$ and $\boldsymbol{R}_2$ of frame $D-u_1v_1w_1$, frame $D-u_2v_2w_2$ with respect to frame $O-xyz$ can be described by rotating about y-axis with $\theta_{1,1}$ angle and u-axis with $\theta_{1,2}$ angle respectively, which are expressed as

$$\boldsymbol{R}_1=\begin{bmatrix} c\theta_{1,1} & 0 & s\theta_{1,1} \\ 0 & 1 & 0 \\ -s\theta_{1,1} & 0 & c\theta_{1,1} \end{bmatrix}, \boldsymbol{R}_2=\begin{bmatrix} 1 & 0 & 0 \\ 0 & c\theta_{1,2} & -s\theta_{1,2} \\ 0 & s\theta_{1,2} & c\theta_{1,2} \end{bmatrix} \tag{1}$$

where c and s denote cosine and sine, respectively.

The relationship between frame $D-uvw$, frame $D-u_1v_1w_1$ and $D-u_2v_2w_2$ frame can be described as

$$\boldsymbol{u}=\boldsymbol{R}_1\boldsymbol{x},\ \ \boldsymbol{w}=(\boldsymbol{R}_1\boldsymbol{x})\times(\boldsymbol{R}_2\boldsymbol{y}),\ \ \boldsymbol{v}=\boldsymbol{w}'\boldsymbol{u} \tag{2}$$

where $\boldsymbol{x}$, and $\boldsymbol{y}$ are the unit axial vectors of frame $O-xyz$, and $\boldsymbol{u}$, $\boldsymbol{v}$ and $\boldsymbol{w}$ represent the unit axial vectors of reference frame $D-uvw$, respectively.

Therefore, the rotational matrix $\boldsymbol{R}$ of frame $D-uvw$ with respect to frame $O-xyz$ is formulated as follows.

$$\boldsymbol{R}=[\boldsymbol{u}\quad\boldsymbol{v}\quad\boldsymbol{w}]=\frac{1}{\sqrt{c^2\theta_{1,2}+c^2\theta_{1,1}s^2\theta_{1,2}}}\begin{bmatrix} c\theta_{1,1} & s\theta_{1,1}c\theta_{1,1}s\theta_{1,2} & s\theta_{1,1}c\theta_{1,2} \\ 0 & c\theta_{1,2} & -c\theta_{1,1}s\theta_{1,2} \\ -s\theta_{1,1} & c^2\theta_{1,1}s\theta_{1,2} & c\theta_{1,1}c\theta_{1,2} \end{bmatrix} \tag{3}$$

Supposed the angles φ_x and φ_y that plate I rotates about x and y-axis are known, the direction vector $\boldsymbol{w}$ of plate I is determined, and the input angles $\theta_{1,1}$ and $\theta_{1,2}$ can be calculated by Eq. (3). For the 1st $\underline{\mathrm{R}}(\mathrm{RU})^2$ limb, frame $D-uvw$ can be obtained by rotating the limb about v_1-axis with $\theta_{1,1}$ and rotating about the other axis of U joint with $\theta_{2,1}$. For the 2nd $\underline{\mathrm{R}}(\mathrm{RU})^2$ limb, frame $D-uvw$ is derived by

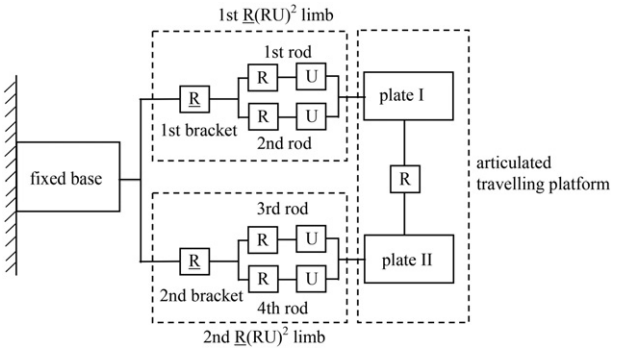

Fig. 1. Topology structure of the 2-DoF RPM.

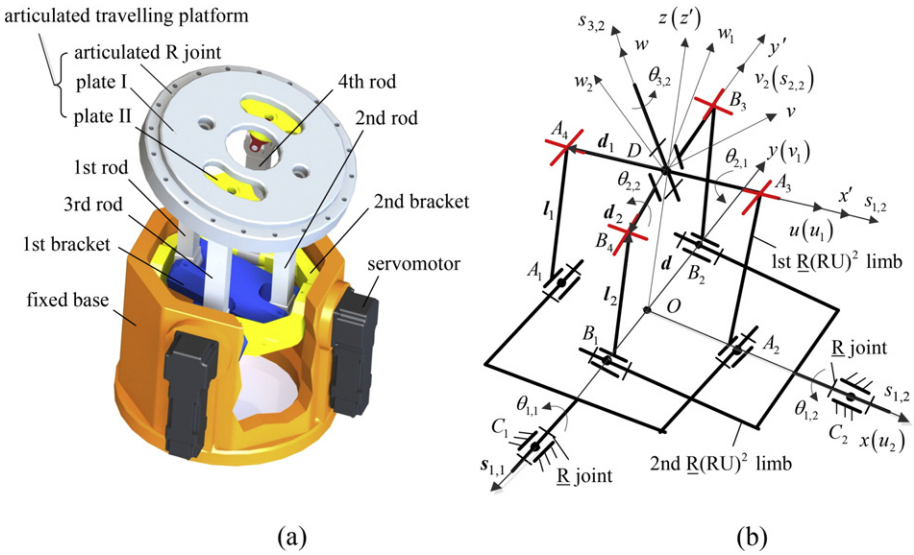

Fig. 2. (a) Virtual prototype and (b) schematic diagram of 2-DoF RPM.

rotating the limb about u_2-axis with $\theta_{1,2}$, then rotating about another axis of U joint with $\theta_{2,2}$, finally rotating about articulated R joint with $\theta_{3,2}$. Therefore, the rotational angle $\theta_{2,1}$ within 1st $\underline{\mathrm{R}}(\mathrm{RU})^2$ limb and $\theta_{2,2}$, $\theta_{3,2}$ within 2nd $\underline{\mathrm{R}}(\mathrm{RU})^2$ limb are determined by

$$\boldsymbol{R} = \boldsymbol{R}_1 \cdot \mathrm{Rot}\left(\boldsymbol{u}_1, \theta_{2,1}\right),\ \boldsymbol{R} = \boldsymbol{R}_2 \cdot \mathrm{Rot}\left(\boldsymbol{v}_2, \theta_{2,2}\right) \cdot \mathrm{Rot}\left(\boldsymbol{w}, \theta_{3,2}\right). \tag{4}$$

3. Stiffness modeling of 2-DoF RPM considering gravitational effects

Based upon the topology structure of the 2-DoF over-constrained RPM, the deformation of plate I caused by an external payload is formed by the deformations of the two $\underline{\mathrm{R}}(\mathrm{RU})^2$ limbs supposing the articulated traveling platform as rigid-body without deformation. According to the mapping relationship of the payload and the deformation, the virtual work principle is employed to formulate the

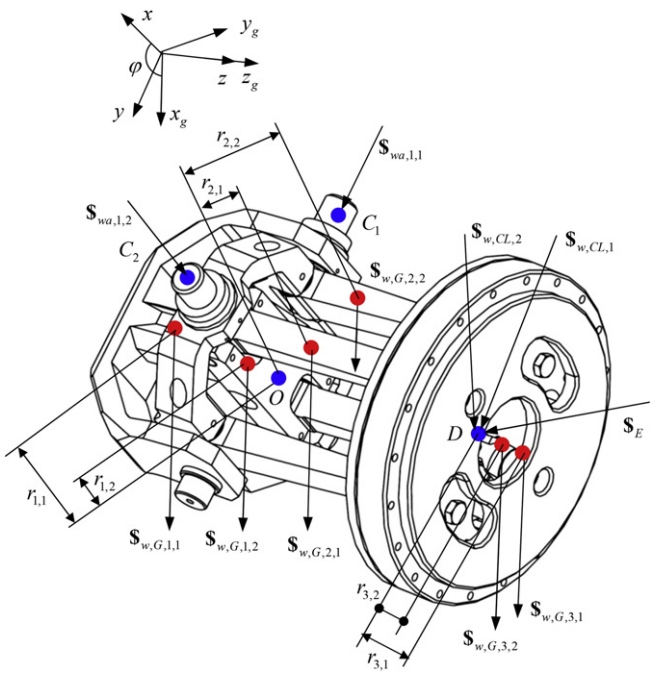

Fig. 3. Free-body diagram of 2-DoF RPM.

stiffness model of the 2-DoF RPM considering gravitational effects, which is implemented by three steps: 1) formulating the twist and wrench mapping models of the two $\underline{\mathrm{R}}(\mathrm{RU})^2$ limbs between their joint spaces and operated spaces considering gravitational effects, respectively, of which the gravitational wrenches are treated as external wrench exerting on the end reference point in the light of static equilibrium; 2) establishing the compliance models of the two $\underline{\mathrm{R}}(\mathrm{RU})^2$ limbs in their joint spaces by means of deformation superposition principle, of which the component compliance in each limb is described by n-DoF ($n \le 6$) virtual springs; and 3) applying deformation compatibility conditions and twist/wrench mapping models into the virtual work equations, the stiffness model of the 2-DoF RPM in the operated space is derived.

3.1. Twist mapping model

Mainly drawing on screw theory, the twist of end reference point D can be represented by a linear combination of the twist of 1-DoF joint in the $\underline{\mathrm{R}}(\mathrm{RU})^2$ limbs. It is mentioned in Ref. [32] that the twist of parallelogram structure is equivalent to the unit screw of permission associated with the 1-DoF R joint. Therefore, the following equations are formulated as

$$\begin{cases} \$_t = \sum_{j_a=1}^{2} \rho_{a,j_a,1} \hat{\$}_{ta,j_a,1} + \sum_{j_c=1}^{4} \rho_{c,j_c,1} \hat{\$}_{tc,j_c,1} \\ \$_t = \sum_{j_a=1}^{3} \rho_{a,j_a,2} \hat{\$}_{ta,j_a,2} + \sum_{j_c=1}^{3} \rho_{c,j_c,2} \hat{\$}_{tc,j_c,2} \end{cases} \tag{5}$$

where $\$_t$ denotes the instantaneous motions (twists) of point D, $\hat{\$}_{ta,j_a,1}$ and $\rho_{a,j_a,1}$ ($\hat{\$}_{tc,j_c,1}$ and $\rho_{c,j_c,1}$) are the jath (jcth) unit screw of permissions (restrictions) and its intensity in the 1st $\underline{\mathrm{R}}(\mathrm{RU})^2$ limb, while $\hat{\$}_{ta,j_a,2}$ and $\rho_{a,j_a,2}$ ($\hat{\$}_{tc,j_c,2}$ and $\rho_{c,j_c,2}$) are the jath (jcth) unit screw of permissions (restrictions) and its intensity in the 2nd $\underline{\mathrm{R}}(\mathrm{RU})^2$ limb and the articulated R joint. Herein, screw of permissions (restrictions) represents the twists permitted (restricted) by the limbs [32].

Taking the generalized inner product on both sides of Eq. (5) with each of $\$_{wa,g_k,k}$ and $\$_{wc,k_c,i}$, leads to

$$\begin{cases} \$_{wa,g_k,k}^{\mathrm{T}} \hat{\$}_t = \rho_{a,g_k,k} \hat{\$}_{wa,g_k,k}^{\mathrm{T}} \hat{\$}_{ta,g_k,k} \\ \$_{wc,k_c,i}^{\mathrm{T}} \hat{\$}_t = \rho_{c,k_c,i} \hat{\$}_{wc,k_c,i}^{\mathrm{T}} \hat{\$}_{tc,k_c,i} \end{cases} \tag{6}$$

where $k = 1, 2$; when $i = 1$, $k_c = 1, 2, 3, 4$; when $i = 2$, $k_c = 1, 2, 3$. $\$_{wa,g_k,k}$, $\hat{\$}_{wa,g_k,k}$ denotes the wrench, unit wrench of actuations associated with the actuated revolute joint and $\$_{wc,k_c,i}$, $\hat{\$}_{wc,k_c,i}$ represents the wrench, unit wrench of constraints, and

$$\$_{wa,g_1,1} = \begin{pmatrix} \mathbf{0} \\ \mathbf{s}_{1,1} \end{pmatrix}, \$_{wa,g_2,2} = \begin{pmatrix} \mathbf{0} \\ \mathbf{s}_{2,2} \times \mathbf{s}_{3,2} \end{pmatrix}, \$_{wc,1,1} = \begin{pmatrix} -\mathbf{s}_{1,1} \times \mathbf{s}_{1,2} \\ \mathbf{0} \end{pmatrix}, \$_{wc,2,1} = \begin{pmatrix} \mathbf{s}_{1,1} \\ \mathbf{0} \end{pmatrix}, \$_{wc,3,1} = \begin{pmatrix} \mathbf{s}_{1,2} \\ \mathbf{0} \end{pmatrix},$$
$$\$_{wc,4,1} = \begin{pmatrix} \mathbf{0} \\ \mathbf{s}_{1,1} \times \mathbf{s}_{2,1} \end{pmatrix}, \$_{wc,1,2} = \begin{pmatrix} -\mathbf{s}_{1,1} \times \mathbf{s}_{1,2} \\ \mathbf{0} \end{pmatrix}, \$_{wc,2,2} = \begin{pmatrix} \mathbf{s}_{1,1} \\ \mathbf{0} \end{pmatrix}, \$_{wc,3,2} = \begin{pmatrix} \mathbf{s}_{1,2} \\ \mathbf{0} \end{pmatrix}.$$

Rewriting Eq. (6) in matrix form results in

$$\boldsymbol{J}_{CL,i} \$_t = \$_{t,CL,i}, \ i = 1, 2 \tag{7}$$

where $\$_{t,CL,i}$ denotes the deformations of the 1st and 2nd $\underline{\mathrm{R}}(\mathrm{RU})^2$ limb in frame $D - u_1v_1w_1$ and frame $D - u_2v_2w_2$, respectively. And

$$\boldsymbol{J}_{CL,1} = \begin{bmatrix} \mathbf{s}_{1,2}^{\mathrm{T}} & \mathbf{0} \\ \mathbf{s}_{1,1}^{\mathrm{T}} & \mathbf{0} \\ \left(\mathbf{s}_{1,2} \times \mathbf{s}_{1,1}\right)^{\mathrm{T}} & \mathbf{0} \\ \mathbf{0} & \mathbf{s}_{1,1}^{\mathrm{T}} \\ \mathbf{0} & \left(\mathbf{s}_{1,2} \times \mathbf{s}_{1,1}\right)^{\mathrm{T}} \end{bmatrix}, \boldsymbol{J}_{CL,2} = \begin{bmatrix} \mathbf{s}_{1,2}^{\mathrm{T}} / \left(\mathbf{s}_{1,2}^{\mathrm{T}} \cdot \mathbf{s}_{2,2} \times \mathbf{s}_{3,2}\right) & \mathbf{0} \\ \mathbf{s}_{1,1}^{\mathrm{T}} / \left(\mathbf{s}_{1,2}^{\mathrm{T}} \cdot \mathbf{s}_{2,2} \times \mathbf{s}_{3,2}\right) & \mathbf{0} \\ \left(\mathbf{s}_{1,2} \times \mathbf{s}_{1,1}\right)^{\mathrm{T}} / \left(\mathbf{s}_{1,2}^{\mathrm{T}} \cdot \mathbf{s}_{2,2} \times \mathbf{s}_{3,2}\right) & \mathbf{0} \\ \mathbf{0} & \mathbf{s}_{1,2}^{\mathrm{T}} / \left(\mathbf{s}_{1,2}^{\mathrm{T}} \cdot \mathbf{s}_{2,2} \times \mathbf{s}_{3,2}\right) \end{bmatrix}.$$

3.2. Wrench mapping model

The wrenches applying on the 2-DoF over-constrained RPM are composed of the external payload, internal payload of actuations/constraints and gravity. Based upon the analysis of wrench mapping model, as shown in Fig. 3, the equation of static equilibrium of the 2-DoF over-constrained RPM at point D can be written as

$$\$_{w,E} + \$_{w,G} = \sum_{k=1}^{2} f_{wa,g_k,k} \hat{\$}_{wa,g_k,k} + \sum_{k_c=1}^{4} f_{wc,k_c,1} \hat{\$}_{wa,k_c,1} + \sum_{k_c=1}^{3} f_{wc,k_c,2} \hat{\$}_{wa,k_c,2} \tag{8}$$

where $\$_{w,E}$ denotes the external wrench exerting on point D, $\$_{w,G}$ is the equivalent gravitational wrench of the 2-DoF RPM applying on point D, $f_{wa,g_k,k}$ is the intensity of actuated wrench and $f_{wc,k_c,1}$ and $f_{wc,k_c,2}$ are the intensities of constrained wrench of 1st and 2nd $\underline{\mathrm{R}}(\mathrm{RU})^2$ limbs, respectively.

$$\$_{w,E}=\begin{bmatrix}\boldsymbol{f}_E\\ \boldsymbol{\tau}_E\end{bmatrix},\ \$_{w,G}=\sum_{j=1}^{2}\sum_{i=1}^{2}\$_{G,i,j},\ \$_{G,1,j}=m_{1,j}g\begin{pmatrix}\boldsymbol{e}_1\\ -\left(\boldsymbol{r}_{1,j}+d\boldsymbol{w}\right)\times\boldsymbol{e}_1\end{pmatrix}$$

$$\$_{G,2,j}=2m_{2,j}g\begin{pmatrix}\boldsymbol{e}_1\\ \left(\boldsymbol{r}_{1,j}-\frac{1}{2}d\boldsymbol{w}\right)\times\boldsymbol{e}_1\end{pmatrix},\ \$_{G,3,j}=m_{3,j}g\begin{pmatrix}\boldsymbol{e}_1\\ \boldsymbol{r}_{3,j}\times\boldsymbol{e}_1\end{pmatrix}$$

where $\boldsymbol{f}_E$ and $\boldsymbol{\tau}_E$ are the external force and torque applying on point D, $\$_{G,i,j}$ is the equivalent gravitational wrench of ith ($i=1,2,3$) component on point D. $m_{i,1}$ represents the mass of the 1st bracket, the 1st rod (2nd rod), and plate I. Similarly, $m_{i,2}$ is the mass of the 2nd bracket, the 3rd rod (4th rod), and plate II. $\boldsymbol{r}_{1,j}$ is the vector from mass center of the 1st bracket or the 2nd bracket to point O, and $\boldsymbol{r}_{2,j}$ is the vector from mass center of the 1st rod (2nd rod) or the 3rd rod (4th rod) to the center of U joint. $\boldsymbol{r}_{3,j}$ denotes the vector between mass center of the articulated traveling plate and point D.

Rewriting Eq. (8) in matrix form leads to

$$\$_w=\boldsymbol{J}_{CL,i}^{\mathrm{T}}\$_{w,CL,i},\ i=1,2 \tag{9}$$

where $\$_w=\$_{w,E}+\$_{w,G}$, $\$_{w,CL,1}=\$_{wa,1,1}+\sum_{k_c=1}^{4}\$_{wc,k_c,1}$, $\$_{w,CL,2}=\$_{wa,1,2}+\sum_{k_c=1}^{3}\$_{wc,k_c,2}$.

It is found out from the wrench mapping analysis that two actuated wrenches and four constrained wrenches are applying to the articulated traveling platform. The constrained wrenches offered by 1st $\underline{\mathrm{R}}(\mathrm{RU})^2$ limb include three force screws along the x, y and z-axes and one moment screw about z-axis while the constrained wrenches from 2nd $\underline{\mathrm{R}}(\mathrm{RU})^2$ limb consist of three force screws along the x, y and z-axes. It is obvious that the three force screws are overconstrained wrenches which have been taken into account respectively in the mapping matrices of 1st and 2nd $\underline{\mathrm{R}}(\mathrm{RU})^2$ limbs to end reference.

3.3. Stiffness model

According to Sections 3.1 and 3.2, the virtual work equation can be written as follow

$$\$_t^{\mathrm{T}}\$_{w,D}=\$_{t,CL,1}^{\mathrm{T}}\$_{w,CL,1}+\$_{t,CL,2}^{\mathrm{T}}\$_{w,CL,2}. \tag{10}$$

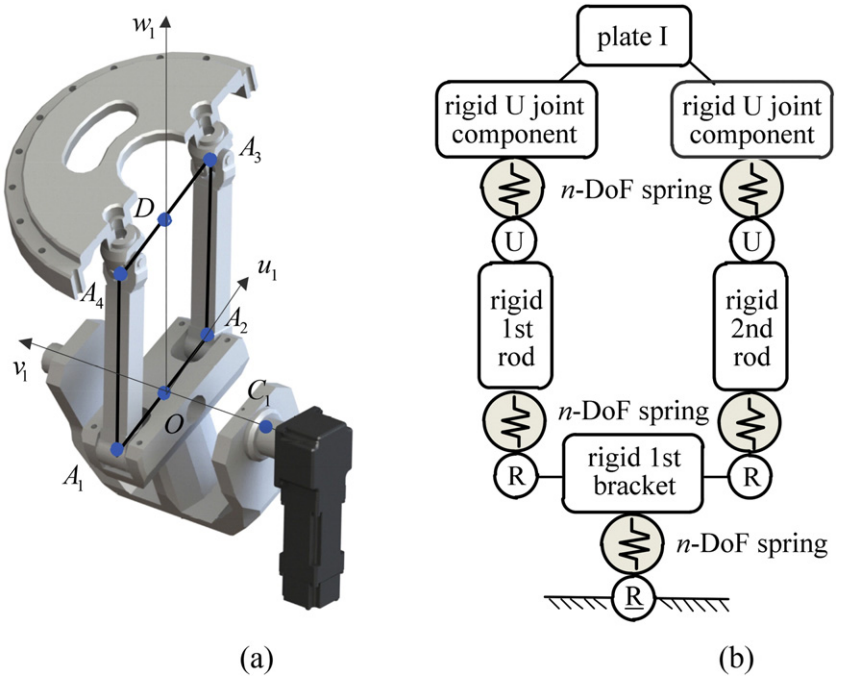

Fig. 4. (a) Virtual prototype and (b) equivalent elastic model of the 1st $\underline{\mathrm{R}}(\mathrm{RU})^2$ limb.

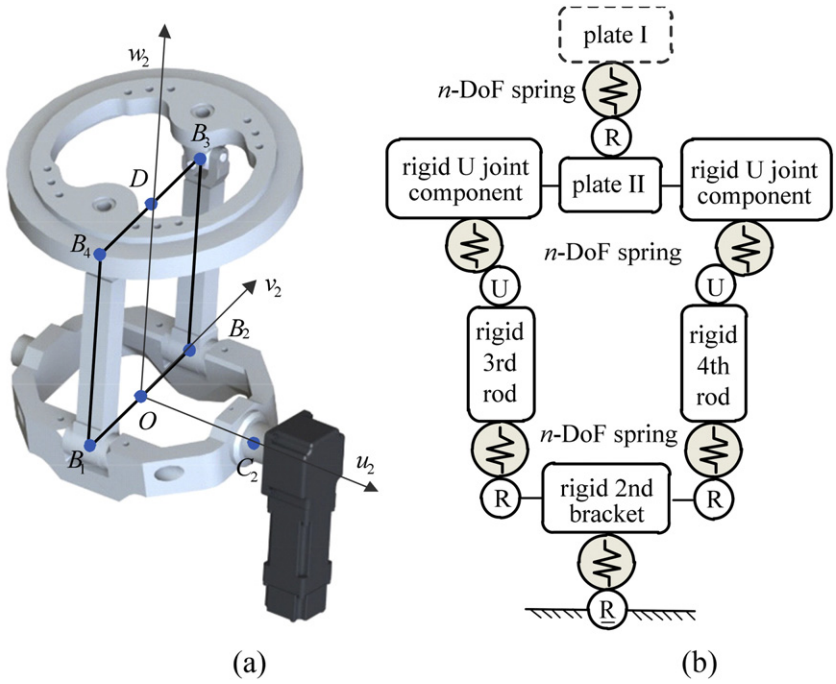

Fig. 5. (a) Virtual prototype and (b) equivalent elastic model of the 2nd $\underline{\mathrm{R}}(\mathrm{RU})^2$ limb.

Based upon aforementioned twist and wrench mapping models, the stiffness model of 2-DoF RPM can be formulated in the light of Hook's Law. Substituting Eqs. (7) and (9) into Eq. (10),

$$\boldsymbol{K} = \sum_{i=1}^{2} \boldsymbol{J}_{CL,i}^{\mathrm{T}} \boldsymbol{K}_{CL,i} \boldsymbol{J}_{CL,i} \tag{11}$$

where $\boldsymbol{K}$ denotes the stiffness matrix of 2-DoF over-constrained RPM, and $\boldsymbol{K}_{CL,i}$ is the stiffness matrices of the 1st and 2nd $\underline{\mathrm{R}}(\mathrm{RU})^2$ limbs in the joint space, respectively.

Considering passive joints within 1st and 2nd $\underline{\mathrm{R}}(\mathrm{RU})^2$ limbs, the rank of $\boldsymbol{K}_{CL,1}$ is 5 and that of $\boldsymbol{K}_{CL,2}$ is 4 which are correspondence to the twist/wrench mapping matrices. Regarding Eq. (11), several assumptions should be made as: 1) the friction and contact deformation within the joints are ignored; 2) the deformations of the components satisfy the linear superposition principle; and 3) the fixed base and the plate I and plate II are regarded as rigid bodies without deformation.

4. Stiffness models of $\underline{\mathrm{R}}(\mathrm{RU})^2$ limbs

In order to formulate the stiffness model of the $\underline{\mathrm{R}}(\mathrm{RU})^2$ limb in their joint space, n-DoF spring is employed to describe the component deformations. Affected by the passive joints, linear or angular stiffness corresponding to the movable axis is zero, resulting in $n \le 6$. It is worth mentioning that the deformations of the $\underline{\mathrm{R}}(\mathrm{RU})^2$ limb can be transferred from fixed base to point D by two roads

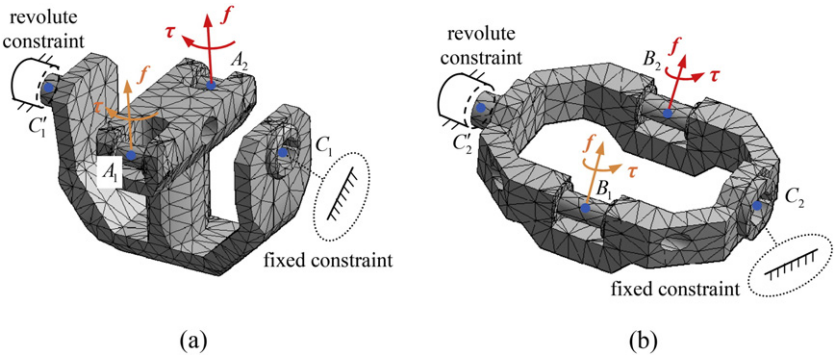

Fig. 6. FEA model of (a) the 1st bracket and (b) the 2nd bracket.

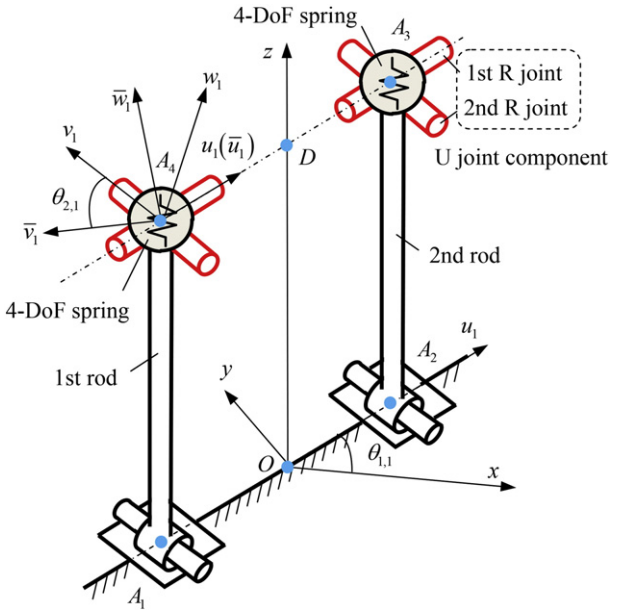

Fig. 7. Equivalent elastic model of the 1st and the 2nd rods.

simultaneously based upon the mechanical principle. Therefore, the stiffness modeling approach of the $\underline{\mathrm{R}}(\mathrm{RU})^2$ limb is implemented by: 1) formulating the compliance of each road by means of deformation superposition principle considering effects of passive joints, 2) establishing the stiffness model of the $\underline{\mathrm{R}}(\mathrm{RU})^2$ limb in their each joint space utilizing Hooke's Law and deformation compatibility conditions.

4.1. The 1st $\underline{\mathrm{R}}(\mathrm{RU})^2$ limb

As shown in Fig. 4a, the equivalent elastic model of the 1st $\underline{\mathrm{R}}(\mathrm{RU})^2$ limb demonstrates the deformation of point D is determined by road $C_1OA_1A_4D$ and road $C_1OA_2A_3D$ simultaneously. It is shown in Fig. 4b that the compliance model at point $A_4(A_3)$ includes the contribution of 1st bracket, 1st (2nd) rod and U joint components.

$$\boldsymbol{C}_{A_4} = \boldsymbol{C}_{1,1} + \boldsymbol{C}_{3,1} + \boldsymbol{C}_{5,1},\ \boldsymbol{C}_{A_3} = \boldsymbol{C}_{2,1} + \boldsymbol{C}_{4,1} + \boldsymbol{C}_{6,1} \tag{12}$$

where $\boldsymbol{C}_{1,1}$ denotes the compliance matrix of the 1st bracket at point A_4 in frame $D - u_1v_1w_1$, $\boldsymbol{C}_{2,1}$ is the compliance matrix of the 1st bracket at point A_3 in frame $D - u_1v_1w_1$, $\boldsymbol{C}_{3,1}$ and $\boldsymbol{C}_{4,1}$ are the compliance matrices of the 1st rod and the 2nd rod in frame $D - u_1v_1w_1$, respectively, and $\boldsymbol{C}_{5,1}$ and $\boldsymbol{C}_{6,1}$ are the compliance matrices of U joint components in frame $D - u_1v_1w_1$.

Since the compliance matrices of 1st (2nd) rod and U joint components are referred to point $A_4(A_3)$, $\boldsymbol{C}_{3,1}(\boldsymbol{C}_{4,1})$ and $\boldsymbol{C}_{5,1}(\boldsymbol{C}_{6,1})$ can be directly applied to Eq. (12). For the 1st bracket, if connecting point $A_4(A_3)$ to point $A_1(A_2)$ by a rigid part and applying a wrench to point $A_4(A_3)$, the deformation twist at point $A_4(A_3)$ is composed of deformation of point $A_1(A_2)$ and the rigid motion of the rigid part, resulting in

$$\boldsymbol{C}_{1,1} = \boldsymbol{T}_{1,1}\overline{\boldsymbol{C}}_{1,1}\boldsymbol{T}_{1,1}^{\mathrm{T}},\ \boldsymbol{C}_{2,1} = \boldsymbol{T}_{2,1}\overline{\boldsymbol{C}}_{2,1}\boldsymbol{T}_{2,1}^{\mathrm{T}} \tag{13}$$

where $\overline{\boldsymbol{C}}_{1,1}(\overline{\boldsymbol{C}}_{2,1})$ represents the compliance matrix at point $A_1(A_2)$, $\boldsymbol{T}_{1,1}(\boldsymbol{T}_{1,2})$ is the transformation matrix of point $A_1(A_2)$ to point $A_4(A_3)$, and $\boldsymbol{T}_{1,1} = \boldsymbol{T}_{2,1} = \begin{bmatrix} \boldsymbol{E}_3 & [-\boldsymbol{l}_1\times] \\ \boldsymbol{0} & \boldsymbol{E}_3 \end{bmatrix}$. Herein, $\boldsymbol{E}_3$ denotes 3×3 unit matrix, $[\boldsymbol{l}_1\times]$ is the skew symmetrical matrix relating to vector $\boldsymbol{l}_1$ from point $A_1(A_2)$ to point $A_4(A_3)$.

Table 1
Dimensional parameters and maximum rotating angles of the 2-DoF over-constrained RPM.

d_1(mm)	d_2(mm)	l_1(mm)	l_2(mm)	$\varphi_{\max}(^\circ)$
60	65	167.5	167.5	45

Table 2
Diagonal elements of component compliance matrix in 1st $\underline{\mathrm{R}}(\mathrm{RU})^2$ limb.

	Linear compliance ($(\mu m/N) \times 10^{-3}$)			Angular compliance $(rad/(N \cdot m)) \times 10^{-6}$		
	c_{11}	c_{22}	c_{33}	c_{44}	c_{55}	c_{66}
$\boldsymbol{C}_{1,1}$	48.873	967.21	2.110	0.363	∞	0.0252
$\boldsymbol{C}_{2,1}$	48.564	973.10	4.109	0.298	∞	0.0235
$\boldsymbol{C}_{3,1}(\boldsymbol{C}_{4,1})$	∞	97.176	1.531	0.0286	∞	0.00172
$\boldsymbol{C}_{5,1}(\boldsymbol{C}_{6,1})$	0.0238	0.0486	0.0546	∞	∞	0.00287

Based upon the Hooke's law and deformation compatibility conditions, the following equation is formulated.

$$\boldsymbol{C}_{A_i}\$_{w,A_i} = \$_{t,A_i},\ \$_{t,D} = \boldsymbol{T}_{A_i}\$_{t,A_i},\ i = 3,4 \tag{14}$$

where $\boldsymbol{T}_{A_i} = \begin{bmatrix} \boldsymbol{E}_3 & (-1)^i[\boldsymbol{d}_1\times] \\ \boldsymbol{0} & \boldsymbol{E}_3 \end{bmatrix}$, $\boldsymbol{d}_1$ is the vector from point D to point A_4 in frame $D - u_1v_1w_1$ as shown in Fig. 2.

Bearing in mind the virtual work principle, the virtual work equation of the 1st $\underline{\mathrm{R}}(\mathrm{RU})^2$ limb at point D is established as

$$\$_{t,CL,1}^{\mathrm{T}}\$_{w,CL,1} = \$_{t,A_3}^{\mathrm{T}}\$_{w,A_3} + \$_{t,A_4}^{\mathrm{T}}\$_{w,A_4}. \tag{15}$$

Substituting Eqs. (12)–(14) into Eq. (15), the stiffness matrix of the 1st $\underline{\mathrm{R}}(\mathrm{RU})^2$ limb in frame $D - u_1v_1w_1$ can be formulated as

$$\boldsymbol{K}_{CL,1} = \sum_{i=3}^{4} \boldsymbol{T}_{A_i}^{-\mathrm{T}}\boldsymbol{C}_{A_i}^{-1}\boldsymbol{T}_{A_i}^{-1}. \tag{16}$$

4.2. The 2nd $\underline{\mathrm{R}}(\mathrm{RU})^2$ limb

The equivalent elastic model of the 2nd $\underline{\mathrm{R}}(\mathrm{RU})^2$ limb is shown in Fig. 5. Similar with the stiffness modeling of 1st $\underline{\mathrm{R}}(\mathrm{RU})^2$ limb, the stiffness matrix of the 2nd $\underline{\mathrm{R}}(\mathrm{RU})^2$ limb in frame $D - u_2v_2w_2$ considering the effect of articulated R joint is calculated as

$$\boldsymbol{K}_{CL,2} = \sum_{i=3}^{4} \boldsymbol{T}_{CL,2}^{-\mathrm{T}}\boldsymbol{T}_{B_i}^{-\mathrm{T}}\boldsymbol{C}_{B_i}^{-1}\boldsymbol{T}_{B_i}^{-1}\boldsymbol{T}_{CL,2}^{-1} + \boldsymbol{T}_{CL,2}^{-\mathrm{T}}\boldsymbol{C}_{aR}^{-1}\boldsymbol{T}_{CL,2}^{-1} \tag{17}$$

where $\boldsymbol{C}_{B_i}$ denotes the compliance matrices at point B_i $(i = 3, 4)$, $\boldsymbol{T}_{B_i}$, $\boldsymbol{T}_{CL,2}$ are the deformation compatibility conditions of plate II and articulated R joint, respectively. $\boldsymbol{C}_{aR}$ is the compliance matrix of articulated R joint. And

$$\boldsymbol{C}_{B_3} = \boldsymbol{C}_{1,2} + \boldsymbol{C}_{3,2} + \boldsymbol{C}_{5,2},\ \boldsymbol{C}_{B_4} = \boldsymbol{C}_{2,2} + \boldsymbol{C}_{4,2} + \boldsymbol{C}_{6,2}$$
$$\boldsymbol{T}_{B_i} = \begin{bmatrix} \boldsymbol{E}_3 & (-1)^i[\boldsymbol{d}_2\times] \\ \boldsymbol{0} & \boldsymbol{E}_3 \end{bmatrix},\ \boldsymbol{T}_{CL,2} = \begin{bmatrix} \boldsymbol{E}_5 & \boldsymbol{0}_{5\times1} \\ \boldsymbol{0}_{1\times5} & 0 \end{bmatrix}$$

where $\boldsymbol{C}_{1,2}$ denotes the compliance matrix of the 2nd bracket at point B_4 in frame $D - u_2v_2w_2$, $\boldsymbol{C}_{2,2}$ represents the compliance matrix of the 2nd bracket at point B_3 in frame $D - u_2v_2w_2$, $\boldsymbol{C}_{3,2}$ *and* $\boldsymbol{C}_{4,2}$ are the compliance matrices of the 3rd rod and the 4th rod in frame $D - u_2v_2w_2$, respectively, and $\boldsymbol{C}_{5,2}$ *and* $\boldsymbol{C}_{6,2}$ are the compliance matrices of U joints in frame $D - u_2v_2w_2$. $\boldsymbol{d}_2$ is the vector of point D to point B_4 in frame $D - u_2v_2w_2$. Similar to 1st $\underline{\mathrm{R}}$(RU)2 limb,

$$\boldsymbol{C}_{1,2} = \boldsymbol{T}_{1,2}\overline{\boldsymbol{C}}_{1,2}\boldsymbol{T}_{1,2}^{\mathrm{T}},\ \boldsymbol{C}_{2,2} = \boldsymbol{T}_{2,2}\overline{\boldsymbol{C}}_{2,2}\boldsymbol{T}_{2,2}^{\mathrm{T}} \tag{18}$$

herein, $\overline{\boldsymbol{C}}_{1,2}(\overline{\boldsymbol{C}}_{2,2})$ denotes the compliance matrix of the 2nd bracket at point $B_1(B_2)$, $\boldsymbol{T}_{1,2}(\boldsymbol{T}_{2,2})$ is the transformation matrix of point $B_1(B_2)$ to point $B_3(B_4)$, $\boldsymbol{T}_{1,2} = \boldsymbol{T}_{2,2} = \begin{bmatrix} \boldsymbol{E}_3 & [-\boldsymbol{l}_2\times] \\ \boldsymbol{0} & \boldsymbol{E}_3 \end{bmatrix}$, and $\boldsymbol{l}_2$ is the vector from point $B_1(B_2)$ to point $B_3(B_4)$.

Table 3
Non-diagonal elements of component compliance matrix in 1st $\underline{\mathrm{R}}(\mathrm{RU})^2$ limb.[a]

	c_{12} (c_{21})	c_{14} (c_{41})	c_{24} (c_{42})	c_{25} (c_{52})	c_{34} (c_{43})	c_{15} (c_{52})	c_{35} (c_{53})	c_{16} (c_{61})	c_{26} (c_{62})
$\boldsymbol{C}_{1,1}$	−0.0026	0	0.0057	0	0.0049	0.0047	0.0034	−0.0023	−0.0026
$\boldsymbol{C}_{2,1}$	−0.0028	0	0.0053	0	0.0050	0.0042	0.0033	−0.0019	−0.0027
$\boldsymbol{C}_{3,1}$ $(\boldsymbol{C}_{4,1})$	0	0	0.021	0	0	0.029	0	0	0
$\boldsymbol{C}_{5,1}$ $(\boldsymbol{C}_{6,1})$	0	0	0	0	−0.0006	0	0.0007	0	0

[a] The elements not listed are 0. Units are either $(m/N) \times 10^{-6}$ or $(rad/(N \cdot m)) \times 10^{-6}$.

Table 4
Diagonal elements of component compliance matrix in 2nd $\underline{R}(RU)^2$ limb.

	Linear compliance ((μm/N) × 10^{-3})			Angular compliance (rad/(N · m)) × 10^{-6}		
	c_{11}	c_{22}	c_{33}	c_{44}	c_{55}	c_{66}
$\boldsymbol{C}_{1,2}$	53.368	6.929	0.123	∞	0.0157	0.0316
$\boldsymbol{C}_{2,2}$	53.368	6.929	0.123	∞	0.0157	0.0316
$\boldsymbol{C}_{3,2}(\boldsymbol{C}_{4,2})$	18.834	∞	0.104	∞	0.00236	0.00917
$\boldsymbol{C}_{5,2}$	0.0238	0.0486	0.0546	∞	∞	0.00287

5. Compliance matrices of components

In this section, the compliance matrices of required components can be derived by means of FEA software since the components with irregular shapes are difficult to be described and analyzed analytically. The process is implemented by: 1) obtaining 6 × 6 compliance matrix with FEA software by applying forces and moments on the output point of components, and 2) formulating accurate compliance matrix considering the effect of passive joints in the $\underline{R}(RU)^2$ limbs, which is demonstrated by n-DoF ($n \le 6$) spring illustrated in Figs. 4 and 5.

5.1. Compliance matrix of 1st and 2nd brackets

As shown in Fig. 6, the 1st and the 2nd brackets have one input point and two output point, respectively. What's more, symmetrical parts connecting to the fixed base with revolute joint to increase stability are implemented. According to the geometry of the 1st (2nd) bracket, fixed constraint is applied to input point C_1 (C_2) while revolute constraint is added to point C_1' (C_2'). Taking compliance matrix at point A_1 as example, unit force/moment along/about u_1, v_1, and w_1-axes is exerting to point A_1 and the compliance matrix is formulated as

$$\overline{\boldsymbol{C}}_{1,1} = \begin{bmatrix} \Delta_{pu1,fu1} & \Delta_{pu1,fv1} & \cdots & \Delta_{pu1,\tau w1} \\ \Delta_{pv1,fu1} & \Delta_{pv1,fv1} & \cdots & \Delta_{pv1,\tau w1} \\ \vdots & \vdots & \cdots & \vdots \\ \Delta_{\alpha w1,fu1} & \Delta_{\alpha w1,fw1} & \cdots & \Delta_{\alpha w1,\tau w1} \end{bmatrix}_{6\times 6} \tag{19}$$

where the ith ($i = 1, 2, \cdots, 6$) column represents linear/angular deformations resulted from unit force/moment. The linear deformations are obtained directly from FEA software while angular deformations are derived from rotation matrix determined by SVD-based solution [24]. With the same approach, compliance matrices at points A_2, B_1 and B_2 are achieved.

Considering the effect of passive R joints and R joints of $\underline{R}(RU)^2$ limb, the angular stiffness about the v_1-axis of the 1st bracket and the x-axis of the 2nd bracket is zero, and then the compliance matrices of the brackets can be described by a 5-DoF virtual spring.

5.2. Compliance matrix of rods

The compliance of the rod can be obtained numerically by FEA software and analytically by regarding the rod as flexible beam element, and the non-zero element of the compliance matrix is

$$\begin{gathered} c_{11} = \frac{l_j^3}{3EI_{vj}},\ c_{22} = \frac{l_j^3}{3EI_{uj}},\ c_{33} = \frac{l_j}{EA_j},\ c_{44} = \frac{l_j}{EI_{uj}},\ c_{55} = \frac{l_j}{EI_{vj}}, \\ c_{15} = c_{51} = \frac{l_j^2}{2EI_{v1}},\ c_{24} = c_{42} = -\frac{l_j^2}{2EI_{u1}},\ j = 1, 2 \end{gathered} \tag{20}$$

where l_j is the length of the 1st (2nd) rod or the 3rd (4th) rod, A_j is the cross-section area, EI_{u1} and EI_{v1} are the bending sectional modules and GI_t is torsional section modulus.

Table 5
Non-diagonal elements of component compliance matrix in 2nd $\underline{R}(RU)^2$ limb.[a]

	c_{12} (c_{21})	c_{23} (c_{32})	c_{24} (c_{42})	c_{15} (c_{51})	c_{34} (c_{43})	c_{35} (c_{53})	c_{16} (c_{61})	c_{26} (c_{62})
$\boldsymbol{C}_{1,2}$	0.011	−0.010	0	0.017	0	−0.023	0.014	0.022
$\boldsymbol{C}_{2,2}$	0.011	−0.010	0	0.017	0	−0.023	0.014	0.022
$\boldsymbol{C}_{3,2}$ ($\boldsymbol{C}_{4,2}$)	0	0	0.024	0.026	0	0	0	0
$\boldsymbol{C}_{5,2}$ ($\boldsymbol{C}_{6,2}$)	0	0	0	0	0.0007	−0.0006	0	0

[a] The elements not listed are 0. Units are either (m/N) × 10^{-6} or (rad/(N · m)) × 10^{-6}.

Table 6
Diagonal elements of compliance matrix of articulated R joint.

	Linear compliance ((μm/N) × 10^{-3})			Angular compliance (rad/(N · m)) × 10^{-6}		
	c_{11}	c_{22}	c_{33}	c_{44}	c_{55}	c_{66}
$\boldsymbol{C}_{aR}$	0.0298	0.0298	0.009	0.0312	0.0312	∞

The method of computing compliance matrices of the 1st and the 2nd rods is the same as compliance matrices of the 3rd and the 4th rods. Taking the 1st and the 2nd rods as example, the equivalent elastic model is as shown in Fig. 7. It is obvious that the 1st and the 2nd rods are components of parallelogram-based structure. The angular stiffness about v_1-axis and linear stiffness along u_1-axis is compensated by the R joints in the parallelogram structure (as described in Ref. [25]), and then the compliance matrices of the 1st and the 2nd rods at point A_4 and A_3 can be described by a 4-DoF virtual spring.

5.3. Compliance matrix of U joint components

As shown in Fig. 5, the U joint is composed of the 1st and 2nd R joints whose axes are perpendicular mutually. The U joint components can be described by a 4-DoF virtual spring considering the effect of the two R joints. The calculation of U joint component in the 1st $\underline{\mathrm{R}}(\mathrm{RU})^2$ limb and the 2nd $\underline{\mathrm{R}}(\mathrm{RU})^2$ limb are the same. Taking U joint component in the 1st $\underline{\mathrm{R}}(\mathrm{RU})^2$ limb as example, the compliance matrix of U joint components can be calculated by the superstition of two R joint components as

$$\boldsymbol{C}_{i,1} = \boldsymbol{C}_{1,i,1} + \boldsymbol{T}_U \boldsymbol{C}_{2,i,1} \boldsymbol{T}_U^{\mathrm{T}},\ i = 5, 6 \tag{21}$$

where $\boldsymbol{C}_{1,i,1}$ denotes the compliance matrix of the 1st R joint in frame $A_j - u_1 v_1 w_1 (j = 3, 4)$, $\boldsymbol{C}_{2,i,1}$ is the compliance matrix of the 2nd R joint in local frame $A_j - \overline{u}_1 \overline{v}_1 \overline{w}_1$ (see Fig. 7), $\boldsymbol{T}_U = \begin{bmatrix} \boldsymbol{R}_{\theta_{2,j}} & \boldsymbol{0} \\ \boldsymbol{0} & \boldsymbol{R}_{\theta_{2,j}} \end{bmatrix}$, and $\boldsymbol{R}_{\theta_{2,j}}$ is the orientation matrix of frame $A_j - \overline{u}_1 \overline{v}_1 \overline{w}_1$ with respect to $D - u_1 v_1 w_1$.

6. Example and discussion

Based upon the kinematic optimal design in Ref. [18], the dimensional parameters and the maximal rotational angles of the 2-DoF over-constrained RPM are given in Table 1. According to the software-based stiffness design and engineering experiences, the inertial parameters are obtained and hereby the virtual prototype of the 2-DoF RPM is established by means of the commercial software. On the basis of the virtual prototype of the 2-DoF RPM, the compliance coefficients, mass and mass centers of components are measured as shown in Tables 2–7.

In order to verify above-mentioned stiffness model considering gravitational effects, the FEA software (ANSYS) analysis is applied to four typical configurations D_1, D_2, D_3 and D_4, whose rotating angles φ_x, and φ_y are (0°, 0°), (45°, 0°), (0°, 45°) and (30°, 30°), respectively. It is worth noting that fixed base and articulated traveling platform are regarded as rigid bodies in order to satisfy the assumptions made in analytical analysis. In addition, component gravity is regarded as distributed force in ANSYS while it is treated as concentrated force applied on mass of center in analytical analysis. Table 8 shows the linear and angular deformations of reference point D in frame $D - xyz$ obtained by theoretical and FEA models. It can be concluded that the variation tendency of the theoretical values is similar to that of the FEA values and the errors are in an acceptable range (within 10%), which indicates the efficiency of the concentrated gravity, and furthermore, validation of theoretical stiffness model.

After verifying the theoretical stiffness model by means of FEA model, the distribution of stiffness and deformation caused by equivalent concentrated gravity in the prescribed workspace can be analyzed explicitly. Fig. 8 demonstrates the linear stiffness k_{px}, k_{py} and k_{pz} and angular stiffness $k_{\alpha x}$, $k_{\alpha y}$ and $k_{\alpha z}$ in frame $O - xyz$. It is easy to find out that: 1) k_{px} and $k_{\alpha x}$ are distributed symmetrical about plane $\varphi_y = 0$. The values of k_{px} gets its maximum when $\varphi_y = 0$, and it gradually decreases with the change of φ_y. When $\varphi_y = 0$,

Table 7
Mass and center of mass of the 2-DoF over-constrained RPM.

	Mass (kg)	Coordinate of central point (mm)		
		u_1	v_1	w_1
1st bracket	6.390	0.95	−0.8	−209.83
2nd bracket	2.839	−4.07	0	−173.89
1st rod (2nd rod)	0.607	−60(60)	0	−96.46
3rd rod (4th rod)	0.861	0	65(−65)	−98.11
1st R joint	0.050	−60(60)	0	0
2nd R joint	0.083	−60(60)	0	12.98
Plate I	3.582	0	0	26.95
Plate II	3.893	0	0	25.95

Table 8
Comparisons between deformations of theoretical and FEA models caused by gravity.

		Δ_{px} ($\times 10^{-5}$ m)	Δ_{py} ($\times 10^{-5}$ m)	Δ_{pz} ($\times 10^{-5}$ m)	$\Delta_{\alpha x}$ ($\times 10^{-6}$ rad)	$\Delta_{\alpha y}$ ($\times 10^{-6}$ rad)	$\Delta_{\alpha z}$ ($\times 10^{-6}$ rad)
D_1	Theoretical	−1.0757	2.8010	0	1.0152	1.0825	−0.0242
	FEA	−1.1301	2.9149	−0.0026	1.0770	1.1348	−0.0256
	Error	4.81%	3.79%		5.74%	4.61%	5.54%
D_2	Theoretical	−1.7057	3.4700	0.0043	0.7463	0.7127	3.1297
	FEA	−1.8562	3.7062	0.0017	0.8115	0.7661	3.3736
	Error	8.10%	6.37%	6.05%	8.03%	6.97%	7.23%
D_3	Theoretical	−1.6620	2.7992	−0.0016	0.6652	0.7839	−4.5189
	FEA	−1.8016	3.0224	−0.0023	0.7050	0.8463	−4.9220
	Error	7.75%	7.38%	3.43%	5.64%	7.37%	8.19%
D_4	Theoretical	−1.4274	3.2338	0.0018	0.1366	0.0926	−0.0168
	FEA	−1.3563	3.2488	0.0019	0.1314	0.0842	−0.0178
	Error	4.98%	4.61%	5.26%	3.80%	9.07%	5.88%

$k_{\alpha u}$ reaches the peak value, it goes down rapidly with the increase of φ_y and starts to rise at around $\varphi_y = \pm 20^{\circ}$ .2) The variations of k_{py} and $k_{\alpha y}$ are similar, which is symmetrical about plane $\varphi_x = 0$. k_{py}, $k_{\alpha y}$ obtain their minimum when $\varphi_x = 0$, and they increase with the change of φ_x. The value of k_{px} is nearly twice bigger than that of k_{py} at the same configuration while the ranges of $k_{\alpha x}$ and $k_{\alpha y}$ are almost the same. 3) The distribution of k_{pz} is axial symmetrical and that of $k_{\alpha z}$ shows plane symmetry. k_{pz} is the biggest when $\varphi_x = 0$ and $\varphi_y = 0$. $k_{\alpha z}$ steadily decreases with the increase of φ_y. The value of k_{pz} is much bigger than k_{px}, k_{py} while $k_{\alpha z}$ is the smallest comparing with the other two angular stiffness.

In fact, the plane symmetrical structure contributes to the plane-symmetrical distribution of the stiffness along/around x-axis and y-axis. The approximately axial symmetrical about z-axis leads to the axial-symmetrical distribution of k_{pz}. As a result, the stiffness distribution, in return, is able to guide the optional design of the mechanism structure. For instance, distribution of k_{pz} shows that there is no need to increase the stiffness along z-axis comparing with k_{px}, and k_{py}. The sharp change of $k_{\alpha x}$ results from the increasing of φ_y indicates that 2nd $\underline{R}(RU)^2$ limb might go through non-monotonous changes, which needs to be specially concerned in the optimal design considering stiffness performance.

Deformation of reference point D caused by equivalent gravity in the prescribed workspace in frame $O - xyz$ is shown in Fig. 9. It can be concluded that: 1) Δ_{px}, and Δ_{py} are distributed symmetrical about planes $\varphi_y = 0$ and $\varphi_x = 0$, respectively. Δ_{px} shows downward changing rule while Δ_{py} steadily goes up with the increase of φ_y and φ_x. The value of Δ_{py} is bigger than Δ_{px} in the same configuration. 2) The distributions of $\Delta_{\alpha x}$ are similar to the change of $k_{\alpha x}$ while $\Delta_{\alpha y}$ shows opposite distribution from $k_{\alpha y}$. The value of $\Delta_{\alpha x}$ is much bigger than that of $\Delta_{\alpha y}$. 3) The distribution of Δ_{pz} and $\Delta_{\alpha z}$ are alike. Both of them are not affected by equivalent gravity when $\varphi_x = 0$,

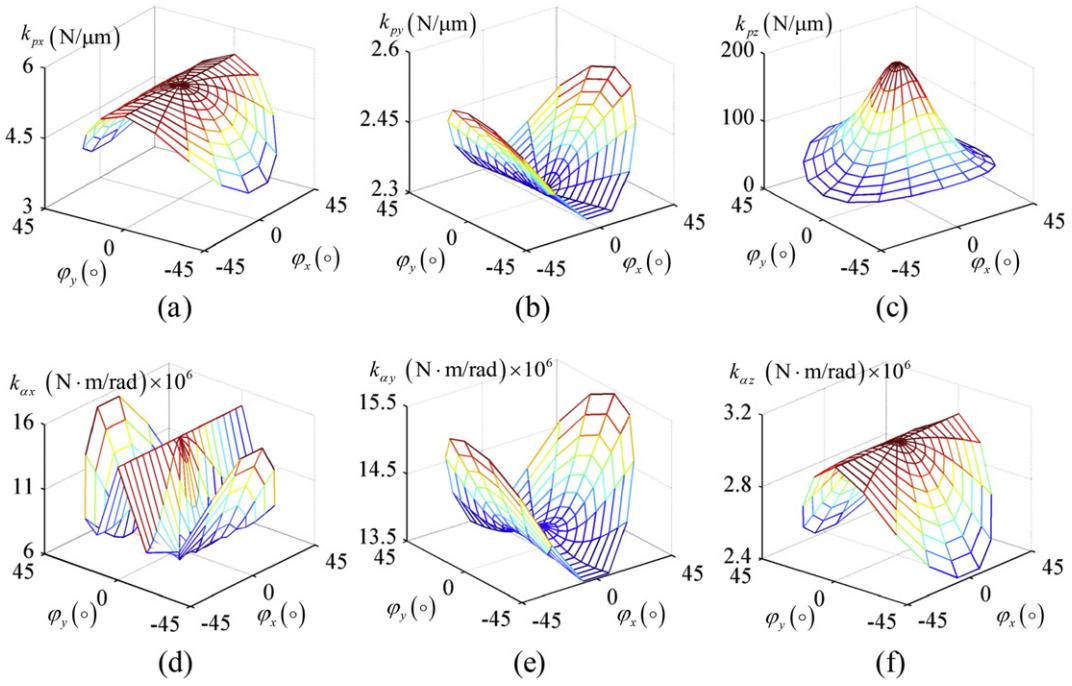

Fig. 8. Stiffness distribution of 2-DoF RPM in frame $O - xyz$.

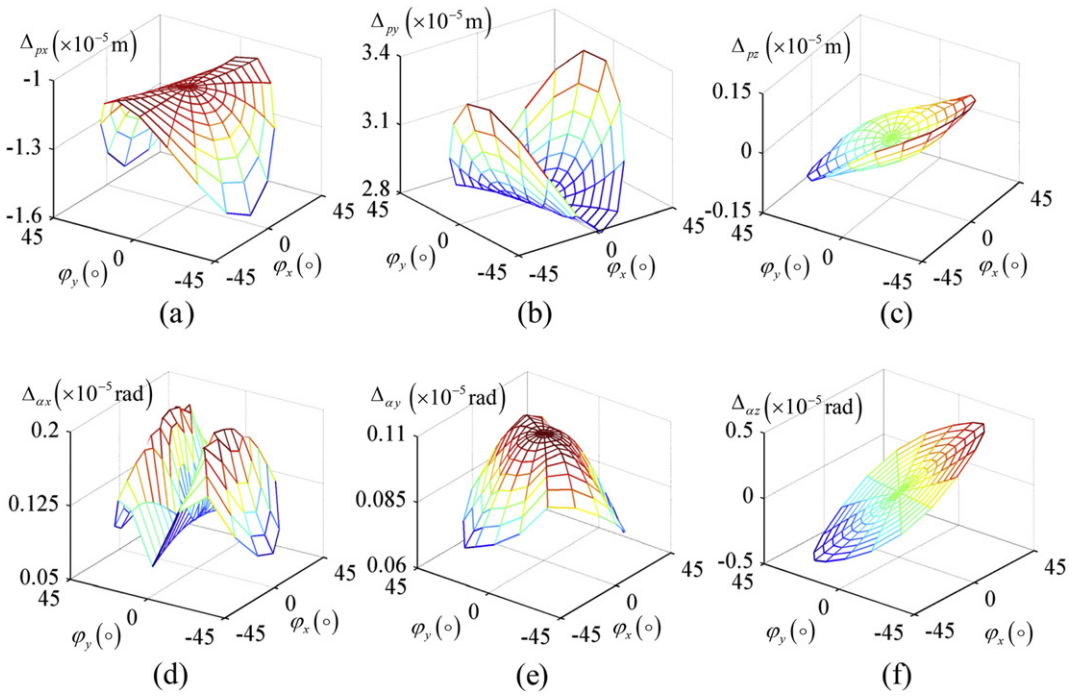

Fig. 9. Deformation of reference point D caused by gravity in frame $O - xyz$.

$\varphi_y = 0$. Δ_{pz} varies with the change of φ_y whereas $\Delta_{\alpha z}$ mainly depends on φ_x. Δ_{pz} and $\Delta_{\alpha z}$ are all smaller than the other linear or angular deformations.

As shown in Fig. 9, the gravity of the 2-DoF over-constrained RPM has some impact on the deformations of reference point D in all directions and it should not be ignored in the stiffness analysis. In fact, the deformation caused by gravity will change when the 2-DoF over-constrained RPM is embedded in different configurations. Therefore, it is a multi-factor analysis including mechanism posture, gravitational effect and stiffness distribution when evaluating stiffness performance of the 2-DoF over-constrained RPM. The results concluded above provide reference for the optimal design issues including: how to arrange the posture of the 2-DoF over-constrained RPM to minimize the effect of gravity, how to achieve compact yet rigid design and how to balance the weight and rigidities of the components.

7. Conclusion

Aiming at the inter-satellite link antenna for 2-DoF tracking mechanisms, this paper carries out the stiffness modeling of a 2-DoF over-constrained RPM with an articulated traveling platform considering gravitational effect. Conclusions are drawn as follows:

(1) The 2-DoF over-constrained RPM is a promising solution for tracking mechanism in the outer space because of the over-constrained structure and the articulated traveling platform. And the stiffness modeling procedure is proposed as firstly formulating the twist/wrench mapping models, then computing stiffness of each limb by the sum of component deformations, and finally applying to the virtual work equation.
(2) Twist/wrenching mapping model of each R(RU)^2 limb to the end reference point is formulated considering the over-constrained property and gravitational effect, in which component gravities are treated as external wrenches applying on the end reference point by static equivalence.
(3) The stiffness model of 1st and 2nd R(RU)^2 limbs in their local reference frames is carried out by deformation superposition principle. Compliance matrices of components are described by n-DoF ($n \le 6$) virtual springs, which takes the effect of passive joints into account to match the twist/wrench mapping models.
(4) The stiffness modeling procedure shows the relationship between component, limbs and mechanism, which is of clear physical meaning and unifies the mechanism performance analysis including kinematic, stiffness, accuracy and dynamic.

Acknowledgments

This research work was supported by the National Natural Science Foundation of China (NSFC) under Grant Nos. 51205278 and 51475321, Tianjin Research Program of Application Foundation and Advanced Technology (Grant No. 15JCZDJC38900).

References

[1] M. Takeuchi, S. Isobe, N. Hamamototoi, S. Ohmori, M. Yamamoto, Experimental advanced mobile satellite communications system in MM-wave and Ka-band using Japan's COMETS, Proc. Global Telecommunications Conference, Orlando, FL, United States Dec 06–Dec 09 1992, pp. 443–446.
[2] D.L. Brandel, W.A. Watson, A. Weinberg, NASA's advanced tracking and data relay satellite system for the years 2000 and beyond, Proc. the IEEE Jul 1990, pp. 1141–1151.
[3] J. Teles, M.V. Samii, C.E. Doll, Overview of TDRS, Adv. Space Res. 16 (12) (1995) 67–76.
[4] J.S. Knogl, P. Henkel, C. Gunther, Precise positioning of a geostationary data relay using LEO satellites, Proc. ESA Workshop on Satellite Navigation Technologies and European Workshop on GNSS Signals and Signal Processing, ESTEC, Noordwijk, Netherlands Sept 14–16 2011, pp. 325–328.
[5] A.G. Roederer, N.E. Jeitseit, G.A.E. Crone, Some European satellite–antenna developments and trends, IEEE Antennas Propag. Mag. 38 (2) (1996) 9–21.
[6] C. M. Gosselin, F. Caron, Two degree-of-freedom spherical orienting device, 1999, US Patent 5966991.
[7] M.J.H. Lum, J. Rosen, M.N. Sinanan, B. Hannaford, Kinematic optimization of a spherical mechanism for a minimally invasive surgical robot, Proc. IEEE International Conference on Robotics and Automation, New Orleans, LA, United States April 26–May 1 2004, pp. 829–834.
[8] M.J.H. Lum, J. Rosen, M.N. Sinanan, B. Hannaford, Optimization of a spherical mechanism for a minimally invasive surgical robot: theoretical and experimental approaches, IEEE Trans. Biomed. Eng. 53 (7) (2006) 1440–1445.
[9] R. Baumann, W. Maeder, D. Glauser, R. Clavel, The PantoScope: a spherical remote-center-of-motion parallel manipulator for force reflection, Proc. IEEE International Conference on Robotics and Automation, Albuquerque, NM, United States Apr 20–25 1997, pp. 718–723.
[10] M.E. Rosheim, G.F. Sauter, New high-angulation omini-direconal sensor mount, SPIE Conference Proceedings, Seattle, WA, 2002.
[11] J. Sdfka, V. Skormin, V. Nikulin, D.J. Nicholson, Omni-Wrist III — a new generation of pointing devices. Part I: laser beam steering devices — mathematical modeling, IEEE Trans. Aerosp. Electron. Syst. 42 (2) (2006) 718–725.
[12] J. Sdfka, V. Skormin, V. Nikulin, et al., Laser communication between mobile platforms, IEEE Trans. Aerosp. Electron. Syst. 45 (1) (2009) 336–346.
[13] J. Sdfka, V. Skormin, Integrated Approach to Electromechanical Design of a Digitally Controlled High Precision Actuator for Aerospace Applications, Proceedings of the 2006 IEEE International Conference on Control Applications Munich, Germany October 4–6 2006, pp. 261–265.
[14] M. Carricato, V. Parenti-Castelli, A novel fully decoupled two-degrees-of-freedom parallel wrist, Int. J. Robot. Res. 23 (6) (2004) 661–667.
[15] R. Di Gregorio, R. Sinatra, Singularity curves of a parallel pointing system, Mechanics 37 (2002) 255–268.
[16] R. Vertechy, V. Parenti-Castelli, Synthesis of 2-DoF spherical fully parallel mechanisms, Adv. Robot Kinematics (2006) 385–394.
[17] K. Wu, J.J. Yu, G.H. Zong, X.W. Kong, A family of rotational parallel manipulators with equal-diameter spherical pure rotation, J. Mech. Robot. 6 (1) (2014) 011008-1–011008-10.
[18] J.J. Yu, X. Dong, X. Pei, X.W. Kong, Mobility and singularity analysis of a class of two degrees of freedom rotational parallel mechanisms using a visual graphic approach, J. Mech. Robot. 4 (4) (2012) 041006-1–041006-10.
[19] G. Gogu, Fully-isotropic over-constrained parallel wrists with two degrees of freedom, Proc. IEEE International Conference on Robotics and Automation, Barcelona, Spain April 18–22 2005, pp. 4014–4019.
[20] A. Cammarata, Optimized design of a large-workspace 2-DoF parallel robot for solar tracking systems, Mech. Mach. Theory 83 (2015) 175–186.
[21] Y.M. Song, B.B. Lian, T. Sun, G. Dong, Y. Qi, H. Gao, A novel 5-DoF parallel manipulator and its kinematic optimization, J. Mech. Robot. 6 (4) (2014) 041008-1–041008-9.
[22] T. Sun, Y.M. Song, H. Gao, Y. Qi, Topology synthesis of a 1-translational and 3-rotational parallel manipulator with an articulated travelling plate, J. Mech. Robot. 7 (3) (2015) (031015-1-03015-9).
[23] Y.M. Song, G. Dong, T. Sun, B.B. Lian, Elasto-dynamic Analysis of a Novel 2-DoF Rotational Parallel Mechanism with an Articulated Travelling Plate, Meccanica (2015) http://dx.doi.org/10.1007/s11012-014-0099-3.
[24] A. Klimchik, D. Chablat, A. Pashkevich, Stiffness modeling for perfect and non-perfect parallel manipulators under internal and external loadings, Mech. Mach. Theory 79 (2014) 1–28.
[25] A. Pashkevich, A. Klimchik, D. Chablat, Enhanced stiffness modeling of manipulators with passive joints, Mech. Mach. Theory 46 (2011) 662–679.
[26] D. Deblaise, X. Hernot, P. Maurine, A systematic analytical method for PKM stiffness matrix calculation, Proc. of the 2006 IEEE International Conference on Robotics and Automation, Florida, USA 2006, pp. 4213–4219.
[27] J. Wu, J.S. Wang, L.P. Wang, T.M. Li, Z. You, Study on the stiffness of a 5-DOF hybrid machine tool with actuation redundancy, Mech. Mach. Theory 44 (2009) 289–305.
[28] A. Cammarata, D. Condorelli, R. Sinatra, An algorithm to study the elastodynamics of parallel kinematic machines with lower kinematic pairs, J. Mech. Robot. 5 (2013) 011004-1–011004-9.
[29] A. Pashkevich, D. Chablat, P. Wenger, Stiffness analysis of overconstrained parallel manipulators, Mech. Mach. Theory 44 (2009) 966–982.
[30] F. Majou, C.M. Gosselin, P. Wenger, D. Chablat, Parametric stiffness analysis of the Orthoglide, Mech. Mach. Theory 42 (2007) 296–311.
[31] A. Taghvaeipour, J. Angeles, L. Lessard, On the elastostatic analysis of mechanical systems, Mech. Mach. Theory 58 (2012) 202–216.
[32] T. Huang, H.T. Liu, D.G. Chetwynd, Generalized Jacobian analysis of lower mobility manipulators, Mech. Mach. Theory 46 (2011) 831–844.